Melanin system composition analyzed by XPS depth profiling

J.V. Paulin , J.D. Mcgettrick , C.F.O. Graeff , A.B. Mostert

PII: S2468-0230(21)00130-9
DOI: https://doi.org/10.1016/j.surfin.2021.101053
Reference: SURFIN 101053

To appear in: *Surfaces and Interfaces*

Received date: 6 January 2021
Revised date: 20 February 2021
Accepted date: 23 February 2021

Please cite this article as: J.V. Paulin , J.D. Mcgettrick , C.F.O. Graeff , A.B. Mostert , Melanin system composition analyzed by XPS depth profiling, *Surfaces and Interfaces* (2021), doi: https://doi.org/10.1016/j.surfin.2021.101053

Highlights

- Comparison of the chemical composition of surface and bulk melanin derivatives.
- The main chemical functions of melanin structure do not change as a function of depth.
- Film processing can slightly change the chemical composition of melanin.
- Similar behavior was found for standard non-functionalized and sulfonated melanin derivatives.

Melanin system composition analyzed by XPS depth profiling

J.V. Paulin[a,b], J.D. Mcgettrick[c], C.F.O. Graeff[a,d], A.B. Mostert[e,*]

[a] São Paulo State University (UNESP), School of Sciences, Postgraduate Program in Materials Science and Technology (POSMAT), Bauru, Brazil.

[b] Swansea University, Department of Physics, Singleton Park, Swansea, SA2 8PP, United Kingdom.

[c] SPECIFIC, Swansea University, College of Engineering, Bay Campus, Fabian Way, Crymlyn Burrows, Swansea, SA1 8EN, United Kingdom.

[d] São Paulo State University (UNESP), School of Sciences, Department of Physics, Bauru, Brazil.

[e] Swansea University, Department of Chemistry, Singleton Park, Swansea, SA2 8PP, United Kingdom.

* Corresponding author:

a.b.mostert@swansea.ac.uk (A. B. Mostert).

Abstract

The melanins are a class of natural pigments ubiquitous throughout the biosphere. These pigments are gaining significant attention as advanced materials due to their biocompatibility, optical and electrical properties. The most common form of melanin, eumelanin, has a well-known problem of insolubility in most common solvents. The insolubility has made standard chemical analysis challenging, leading to researchers opting to use X-Ray photoelectron spectroscopy (XPS). However, standard XPS used on melanins and related materials have been limited to being a surface technique, and hence reported values to date may not reflect the bulk. In this work, we have investigated with XPS depth-profiling method the chemical information of the surface and the bulk of powder and thin-films eumelanin and several melanin derivatives. These latter derivatives are modified melanins designed to overcome the insolubility of the standard systems. Our result indicates that there are only few differences in the chemical composition of the melanin chemical structure between the surface and bulk, for either the powder of film samples. Our results show that a basic surface probe is sufficient to obtain an accurate elemental composition for basic melanin samples. As such, our analysis indicates that XPS characterization is an important characterization of polyindolequinone systems in general such as the melanins and polydopamines.

Graphical abstract XX

Keywords: X-Ray Photoelectron Spectroscopy; Depth-profile XPS, Polyindolequinone; Eumelanin; Melanin derivatives; Polydopamine.

Introduction

The melanins are a ubiquitous pigment found throughout the biosphere and plays many important functional roles in higher-and-lower-order organisms, including humans [1,2]. The two main forms of this class of pigment are eumelanin, the brown-black pigment and is considered the archetypal melanin, and pheomelanin, the red-yellow pigment [1,2]. The melanins are best known for their primary role in the human body, to act as photo protection against harmful UV radiation [3], though they also appear in substantial amounts in other parts of the body including the *substantia nigra* of the brain stem where their function is currently not know but is suspected to aid in neural transmission [4].

In the past couple of years the melanins, more specifically eumelanin, has attracted significant attention as an advanced material for applications in coatings and devices [5]. Eumelanin, or in common parlance, melanin, has several material properties that make it an attractive material: i) biocompatibility [1]; ii) near unity optical absorption with a broad band spectrum [6], iii) ability to chelate and react with large quantities of transition metal ions [7,8]; iv) a stable free radical signal [1]; v) easy processing for creating device-quality thin films [6–16]; and vi) importantly, appears to sustain a solid-state protonic current [19–25] when wetted, though there is still an active debate as to the nature of charge carriers in the dry state [26]. The solid state protonic current has been attributed to a redox reaction, the comproportionation equilibrium [21,23,27] in which the long-range conductivity is regulated by the local concentration of protons and semiquinone free radicals.

Melanin itself is a polyindolequinone system polymerized from two monomers, dihydroxyindole (DHI) and dihydroxyindole carboxylic acid (DHICA) and their various redox states (Figure 1(a)) [1]. These monomers, under oxidative conditions, form a heterogeneous, stacked oligomer system with characteristic properties such as the aforementioned broadband UV-Vis absorbance and stable free radical signals observed via electron paramagnetic resonance [1]. Melanin is thus a bio-macromolecular system with physicochemical properties that are strongly influenced by disorder at several levels of structure, including its basic chemical make-up [1].

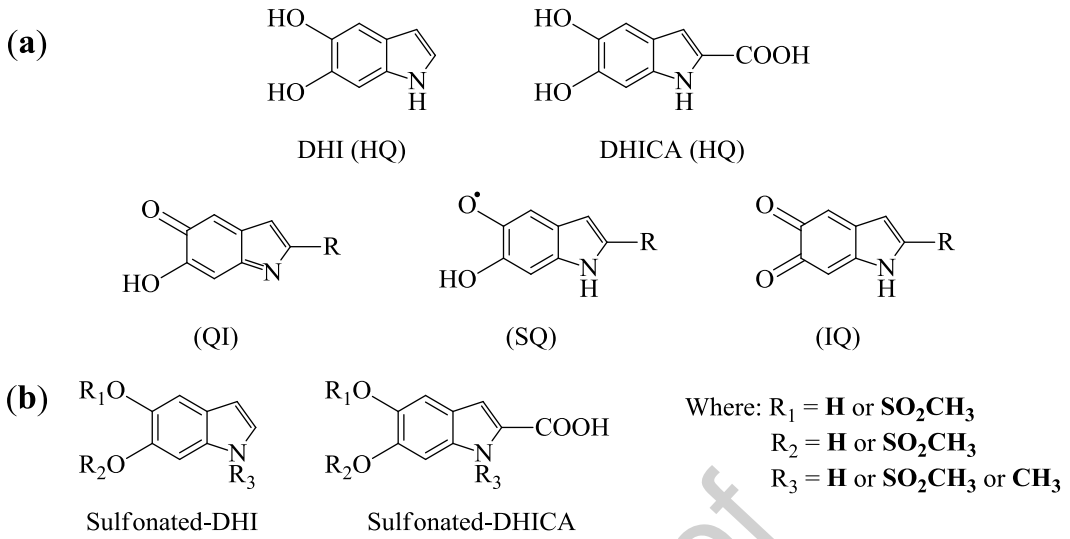

Figure 1. (a) The starting monomers for melanin polymerization. R = H (for DHI-like species) or R = COOH (for DHICA-like species). Furthermore, HQ stands for hydroquinone, QI for quinone imine, SQ for semiquinone and IQ for indolequinone. (b) Proposed building blocks of sulfonated melanins [28].

The structural disorder is well known, and the fact that the stacked oligomeric structure leads to melanin's well-known insolubility has made chemical analysis (e.g., simple elemental analysis) of melanin a notorious problem [1].

One way researchers have dealt with their chemical analysis is to use X-ray photoelectron spectroscopy (XPS) to determine the basic atomic ratios of their samples [12,14,29–32]. The ease of use and the ability to skip the use of solvents and bypass the insolubility problem is a significant benefit. Furthermore, melanin is known to be highly hygroscopic [16,23,33]. Hence using XPS, a technique that is done under vacuum will have the bonus of removing the substantial contribution of physisorbed water, which can skew an elemental analysis.

However, XPS is a surface technique, and the question always remains as to whether the spectra observed is an accurate indication of the bulk of the material, since the upper layers of the material can be modified by the adsorption of CO, water and other molecules from the air or due to partial oxidation under contact with the air. To address this primary issue and investigate whether the use of XPS in recent literature has been legitimate, we present here a depth profile XPS study on melanin and melanin derivatives. The XPS technique has rapidly evolved in recent times, and new spectrometers include "soft etching" argon cluster or fullerene/coronene depth-profiling techniques, enabling the study of organic materials without graphitization. In essence, as a photoelectron scan is obtained, the top surface of the sample is gently burned away with an

ion beam, and the next layer investigated, i.e., the bulk is probed. Given this technique, we believe it is an opportune time to explore melanin materials and see whether there is indeed a difference between the surface and the bulk composition.

We extend our study to multiple kinds of melanin derivatives, including the soluble and sulfonated melanins (Figure 1(b)) [9,28,34–36] as a compare and contrast study with a "standard" synthetic melanin, since the elemental analysis of these materials is not well investigated. These latter melanins have been engineered to overcome the insolubility problem and present interesting properties by themselves, such as homogeneous thin-films production [9,14,37,38], biocompatibility [37], redox activity [18,38], and paramagnetism [9,39]. Furthermore, we investigate the differences between pressed powder samples, which can be considered as pure melanins, and those spin-coated for technological applications. Films are an important morphology since the melanins as a class of material are being incoportated into a wide array of devices in the form of thin films. Hence, thin fims of melanins are an important standard to investigate. As such, melanin films are usually spin-coated out of a solvent, and there is some question as to whether some chemical modification is occurring during this intermediate fabrication step [14].

Experimental

All commercial chemicals were used without further purification.

Synthesis of melanin-derivatives in water:

Previously published methods for synthesis of melanin derivatives were followed [35,40]. In brief, 5 g of 3,4-dihydroxyphenyl-DL-alanine (DL-Dopa; Sigma-Aldrich) were dissolved in 2 L of deionized water. Ammonia (NH_3; Sigma-Aldrich, 28 %) was used to adjusted the mixture to pH 8. The solution was kept under constant stirring and with air bubbling through the solution for 3 days. By keeping the maximum pH at 8 ensured that the ring fission of the indolequinone moieties is kept to a minimum, ensuring a biomimetic material [41]. After 3 days, a concentrated hydrochloric acid (Sigma-Aldrich, 25%) was used to adjust to pH 2 and precipitate the melanin. The aggregated solution was filtered, washed several times using deionized water, and dried overnight under ambient conditions to yield a black powder. This sample is designated as NFMel-I.

0.3 g of DL-Dopa was dissolved in 60 mL of MiliQ water (18 MΩ cm). The pH of the

mixture was adjusted to be between 8 and 10 by the addition of 400 µL of aqueous ammonia (NH_4OH; Synth, 28-30%). The solution was kept stirring in room temperature (27 ºC) and oxygenated using an air pump for three days (sample designation: NFMel-S) or in a 150 mL stainless steel reactor with an internal pressure of 6 atm of industrial oxygen gas for 6 hours (sample designation: NFMel-6P). After this period, the solution was placed in a 3500 MWCO dialysis membrane with MiliQ water as a dialysate medium for approximately four days. Finally, black powder was obtained after dried of the aggregated solution in an oven at 90 °C for two days.

Synthesis of sulfonated-melanin derivatives:

Sulfonated melanin derivatives were made following previous methods as follows [9,34,36]: In 200 mL of DMSO (PA, Vetec, 99.9%), 1.50 g of DL-DOPA and 0.93 g of benzoyl peroxide (Vetec, 75.0-80.0 %) were dissolved in a flask. This mixture was kept under magnetic stirring for 57 days at room temperature (sample designation: SMel) or eleven days in a temperature-controlled silicone bath at 100 °C with a reflux condenser attached to the flask (sample designation: SMel-T). For extraction and purification, the reaction solution was heated at 140 °C to concentrated to ¼ of the initial volume, and then 150 mL of acetonitrile (Synth, 99.5%) was added to the solution. The new solution was allowed to stand for two days. Afterward, it was centrifuged at 2500 rpm for 15 minutes. The precipitate was dried in the oven at 90 °C for two days.

0.45 g of DL-DOPA was dissolved in 60 mL of DMSO. The solution was placed in a 150 mL stainless steel reactor and stirred with 4 atm of O_2 internal pressure for six days (sample designation: SMel-4P) or with 8 atm for three days (sample designation: SMel-8P). The same extraction and purification procedure described for SMel and SMel-T was followed.

Sample preparation

Melanin was analyzed in two different formats: pellet and thin-film. For the pellets, approximately 150 mg of each melanin derivative was crushed to a fine powder and pressed into a pellet with dimensions of 13 mm of diameter and 1 mm of thickness using a standard pellet press under 10 tons of pressure for 5 minutes. Afterward, for XPS analysis, the pellets were broken in small pieces with around 0.3 cm^2.

Melanin thin-films were deposited into glass slides (25 x 25 mm) that were initially

cleaned with a soap solution (Alcanox®), rinsed in water, ultra-sonicated in acetone (15 min) and 2-propanol (15 min). Prior to deposition, the glass was dried with nitrogen flow and treated with UV-ozone (20 min). The films were prepared by two steps spin-coating (1000 rpm for 60 s and 4000 rpm for 30 s) with 30 mg/mL solution. Due to the insolubility of NFMel-I, thin-films are usually made by dispersing the sample in a mixture of distilled water and ammonia (1 H_2O:2 NH_3 %v) [11]. Hence, 30 mg of NFMel-I were dispersed in 1 mL of such mixture, stirred for 1 hour at 50 °C, ultra-sonicated for another 1 hour, and filtered with a 0.45 μm Hydrophobic PTFE filter (Cole-Parmer). Additionally, as NFMel-S and NFMel-6P are water-soluble samples, a less concentrated ammonia solution was used to decrease the possibility of any structural alterations [14,16]. In this case, 30 mg of NFMel-S and NFMel-6P was diluted in 1 mL of a mixture of deionized water and ammonia (3 H_2O:2 NH_3 %v) or 1 mL of deionized water only (1 H_2O:0 NH_3 %v) before following the same procedure from before. For sulfonated melanin derivatives (synthesized in DMSO), 30 mg of the sample were dispersed in 1 mL of anhydrous DMSO (Sigma-Aldrich, ≥ 99.9%), or anhydrous N,N-dimethylformamide (DMF; Sigma-Aldrich, ≥ 99.8%), or anhydrous 1-Methyl-2-pyrrolidone (NMP; Sigma-Aldrich, ≥ 99.5%) stirred for 1 hour at 50 °C and filtered with a 0.45 μm Hydrophobic PTFE filter (Cole-Parmer).

XPS measurements

The XPS was performed on a Kratos Axis Supra using a 225 W AlKα X-rays with an emission current of 15 mA and equipped with a quartz crystal monochromator with a 500 mm Rowland circle. The X-rays typically illuminate a 300 x 700 μm area, with sampling depth being limited by the mean free path of an electron in this energy range to < 10 nm. High-resolution spectra were collected with a pass energy of 40 eV, with the hybrid lens setting that uses both electrostatic and magnetic immersion lenses to collect the photoelectrons, 0.1 eV step size, 1 s dwell time for electron counting at each step, and up to four sweeps depending on the signal/noise ratio. The integral Kratos charge neutralizer was used as an electron source to eliminate differential charging. For depth profiles, XPS spectra were collected after etching by a rastered (3 x 3 mm) Ar_{500}^+ (500 Argon ions) cluster beam for between 0-600 s. By using Argon clusters this soft etching method allows for a gentle elimination of organic material and prevent the common problem of graphitization. A good test for graphitization and stability of the melanins, is to evaluate the melanin sample using the depth-profile analysis with different acceleration voltages, which we do on NFMel-I and SMel with 5 and 10 kV acceleration

voltages. Here it should be noted that the acceleration voltage is for the entire Argon cluster. Hence the energy per atom is significantly less than expected for more classical single ion etching, which otherwise could lead to major changes in the underlying chemistry [42]. By integrating the carbon peak areas, Figure S1 in Supplementary Material, it is possible to observe an increase in the atomic% for both pellets at 10 kV acceleration voltage, which can be understood as the formation of the aforementioned graphite-like structures. Thus, the result indicates that the samples are unstable at such etching energy. Hence, all the measurements were performed with 5 kV to avoid possible degradation effects of the melanin structure. During depth profiling, the excess argon caused pressure in the sample analysis chamber to rise to 3.0×10^{-7} Torr from the instrument base pressure of 4.4×10^{-9} Torr. The integral charge neutralizer was used to limit the build-up of any surface charge.

The analysis was performed in CasaXPS (2.3.17dev6.4k) using the Kratos sensitivity factor library. A Shirley background was used, and mixed Gaussian-Lorentzian peaks, with 30% Lorentzian character (GL(30)), fitted to the raw data. After fitting of the data, the x-axis of all spectra was charge calibrated to the C-C component in the C1s fit at 284.8 eV.

Results and discussion

Synthetic Non-Functionalized Insoluble Melanin Powder

Our study begins with the XPS spectra of the pellet sample labeled NFMel-I, which is a sample made with the standard procedure and are accepted as synthetic versions of melanin [41]. This enables us to obtain a baseline of comparison when we come to compare to the other materials. From the surface high-resolution scans (i.e., time = 0 seconds, Figure 2(a-c)), we estimate the atomic content for carbon (C1s), oxygen (O1s) and nitrogen (N1s) and compare it to the values we would expect for a non-functionalized poly-DHI (NF-DHI) and non-functionalized poly-DHICA (NF-DHICA) systems. In principle, the synthetic melanins should roughly be in between the aforementioned polyindoquinone systems. The atomic percentages and ratios are shown in Table 1 (first three rows) for the pellet surface. The data in Table 1 were renormalized to exclude the pellets contaminants of sulfur (S2p), calcium (Ca2p) and silicon (Si2p) (see Table S1 for each atomic composition) from syntheses solvents impurities and sample handling.

Table 1. The atomic composition (atomic concentration %) and atomic ratios determined from pressed powder pellets of standard synthetic melanin samples.

Samples	**C** (at%)	**O** (at%)	**N** (at%)	**C/N**	**O/N**	**C/O**
NF-DHI (Theoretical)	72.7	18.2	9.1	8	2	4
NF-DHICA (Theoretical)	64.3	29.6	7.1	9	4	2.2
NFMel-I (Pellet surface)	69.1	22.6	8.2	8.4	2.7	3.1
NFMel-I (Pellet bulk)	69.7	19.2	11.1	6.3	1.7	3.6

By comparing the C/O/N contents, it is possible to evaluate that they are within anticipated values, which suggest that these samples are a combination of DHI and DHICA (in fewer amount) monomers. Hence, at the moment, the surface scan result does appear to validate the XPS method for elemental analysis. However, as indicated in the introduction, the surface may still not be a representation of the bulk. To this end, we inspect the resulting depth profile spectra (Figure 2(a-c), time > 0 s).

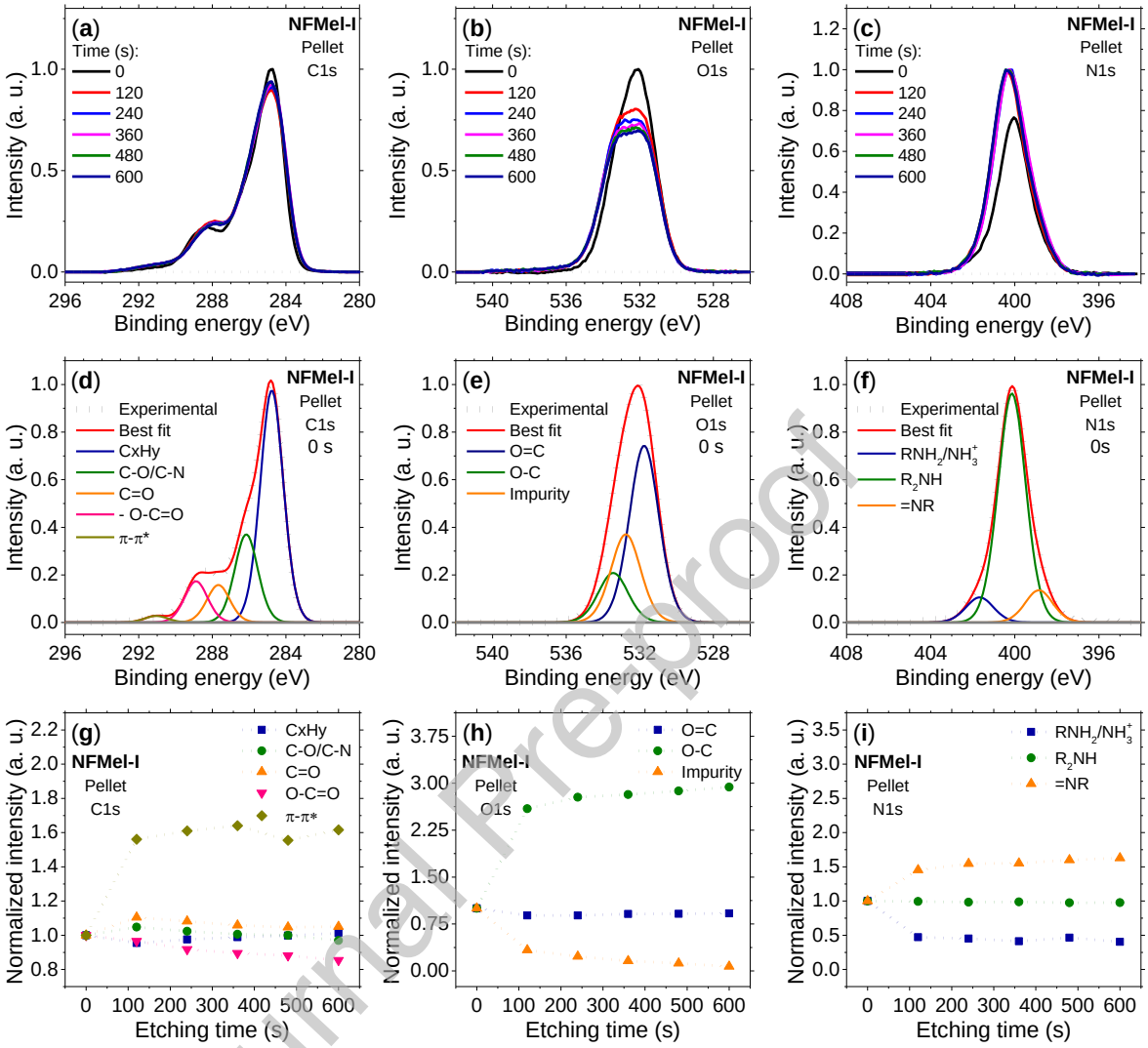

Figure 2. (a-c) High-resolution XPS depth profiling spectra of NFMeI-I pellet. The legends indicate the time since start of depth profiling. 0 seconds is equivalent to a standard surface scan, whereas 600 s (after five etching procedure with 5 kV energy during 120 s each) is considered the pellet bulk. (d-f) High-resolution XPS spectra simulation for a surface pellet of NFMeI-I. The same modeling was applied to the depth profile spectra. (g-i) Functional group distribution as a function of etching time normalized by the surface intensity.

The carbon spectra, Figure 2(a), shows that there are minimal changes with etching, which demonstrate that the underlying carbon chemistry is unchanged between the surface and the bulk. Note that the small variation in intensity at around 284.8 eV could potentially be ascribed as the removal of adventitious carbon. However, one may see that the intensity of O1s spectra, Figure 2(b), decreases of about 9.4%, in area, while N1s, Figure 2(c), increases about 38.8%. The difference in the oxygen spectra could be understood as due to the removal of water trapped

within the macromolecule or the removal of surface impurities. Given that the reported binding energies for H_2O can range from ~533 – 535 eV with outliers to 538 eV (see example in references [43–45]), the presence of water is an unlikely reason. Hence, we ascribe the change to the removal of oxygen impurities.

Regarding the nitrogen behavior, the binding energy is commensurate with that of indole nitrogen, as has been observed for melanin and melanin-like materials [29,30,32]. Therefore, we suggest that the indole nitrogen on the surface is a slightly different chemical species to that which is seen in the bulk, but both are indoles. In fact, the depth profile spectra in Figure 2(c) show that there is a subtle shift to higher binding energy (+ 0.2 eV), which could be understood as changes in the nitrogen atom local charge. Such variation suggests a lower electron density, probably due to the possibility of a more systematic opportunity for non-covalent interactions (like hydrogen bonding) given by a packed structure [46].

With the above, we calculated the atomic percentages and ratios of the pellet bulk (i.e., with 600 s of etching) and the results are shown in Table 1 (last row). The data indicate that the bulk is well within the expected values for a melanin sample, barring the nitrogen content, which is only slightly outside the expected range. Therefore, the depth profile data for the bulk confirms that the surface and the bulk chemical composition of the standard melanin are similar enough to that of a surface scan, which validates and confirms previous elemental analysis done via XPS. It is important to note here that, NFMel-I and, as we will be shown latter, the other melanin samples did not change significantly in relative intensities of the XPS spectra of the constituent atoms as well as binding energy positions of the XPS core-level C(N,O)1s spectra, i.e., the surface (t = 0 s) and the bulk scan (t = 600 s) give the same result, which imply that any possible damage or surface modification provoked by the Ar_{500}^{+} cluster beam can be consider minimal or non-existent, unlike what occurs in semiconducting crystals at higher Ar^{+} energies [47–50].

However, to make the above even more useful for any future work, we now turn to some modeling of the peaks. A representative peak simulation of the high-resolution XPS spectra of C1s, O1s and N1s regions at the pellet surface is shown in Figure 2(d-f). The assigned chemical groups with their respective energies are listed in Table S2 and are compatible with those from the literature [29–32,35]. The same model was a good representative of these three regions for all depth profiled spectra. The only difference was the atomic composition intensity of each peak that is shown in Figure 2(g-i).

There are five carbon species assigned to CxHy, C-O/C-N, C=O, O-C=O and π-π* to fit the C1s region reasonably. The intensity of primary peaks attributed to CxHy, C-O/C-N and C=O species seems not to suffer significant variation with etching time, which is an indicator that the basic melanin indole structure remains the same from the surface to the bulk. On the other hand, a slight decrease in intensity was observed for O-C=O species, whereas π-π* satellite showed a significant increase with etching time. The latter can be an indication of higher strength of extended delocalized electrons from aromatic carbon species in bulk, probably related to the π-π packing in the melanins [51,52]. Moreover, Figure 1(a) shows that the basic monomers of melanin have quinone oxygen/ketones, hydroxy and carboxyl groups (for DHICA species only). Hence, our attributions of two peaks assigned to O=C and O−C species for the fit of the O1s region are in good agreement with the expected chemical composition. These species seem to be consistent across the entire sample, however, with the change in intensities related to the removal of surface impurities, as discussed above. Note that the ratio of ketone/hydroxyl indole groups will not necessarily be one to one, due to the structural disorder and inability to precisely control the oxidation status of the different monomeric species that build up the samples. The N1s regions were fitted with three different indole nitrogen species. Based on the melanin chemical structure, the main species (R_2-NH) is understood as the pyrrole-like nitrogen from the indole structure, while the imine (=NR) functionality as the tautomer quinone imine (QI in Figure 1(a)) and potential non-cyclized structures and polaron species (RNH_2/NH_3^+). It is interesting in the N1s region, is that R_2-NH species do not vary with the etching time, which corroborates the above discussion that the basic melanin is not changed from the surface to the bulk.

Synthetic Non-Functionalized Insoluble Melanin Thin-film

As mentioned previously, melanin thin films possess an important morphology for device applciations, and hence should be investigated. Thin-films for standard synthetic melanins are usually obtained using an ammonia solution to help dissolve the initial powder and improve its adhesion. Still, it can also increase the nitrogen content in the sample [14,16]. Hence, we would like to evaluate if the ammonia would present a more significant effect on the chemical information on the melanin sample, i.e., the stability of the indole ring structure and oxidation state. The corresponding atomic percentages and ratios are given in Table 2 and the resultant XPS spectra can be seen in Figure 3(a-c). Again, the results presented in Table 2 were renormalized to exclude sulfur (S2p), calcium (Ca2p), silicon (Si2p) and sodium (Na1s)

impurities (see Table S3).

Table 2. The atomic composition (atomic concentration %) and atomic ratios determined from the spin-coated thin-films of standard synthetic melanin samples.

Samples	C (at%)	O (at%)	N (at%)	C/N	O/N	C/O
NFMel-I (H_2O+NH_3 film surface)	61.2	26.8	12.0	5.1	2.2	2.3
NFMel-I (H_2O+NH_3 film bulk)	62.9	22.7	14.3	4.4	1.6	2.8

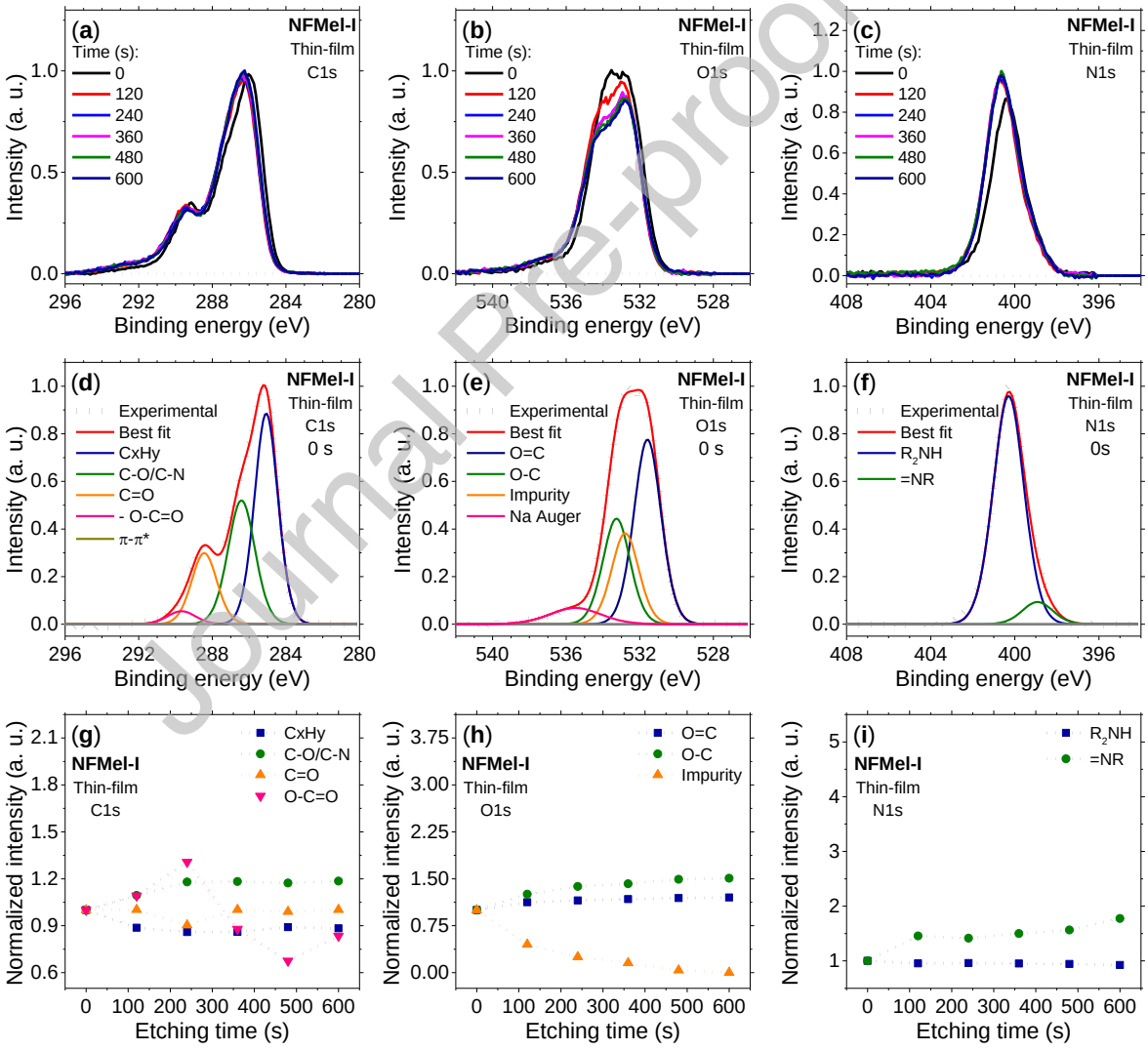

Figure 3. (a-c) C1s, O1s and N1s high-resolution XPS depth profiling for NFMel-I thin-film from standard water and ammonia procedure (H_2O+NH_3). Also indicated in the legends is the time since the start of depth profiling. 0 seconds, in this case, is equivalent to a standard surface

scan. 600 s (equal to 5 different etching with 5 kV energy during 120 s each) represents the thin-film bulk. (d-f) High-resolution XPS spectra simulation of C1s, O1s and N1s regions for a surface thin-film of NFMel-I prepared using standard ammonia procedure (H_2O+NH_3). The same modeling was applied to the depth profile spectra. (g-i) Functional group distribution as a function of etching time normalized by the surface intensity.

The films prepared with the traditional ammonia solutions showed a few divergences to the theoretical values for the surface scans. It is clear that the use of ammonia increases the amount of nitrogen in the film, as shown in a previous study [14]. As a result, the percentage values of carbon and oxygen are also changed. Such alterations could be an indication of adjustment in the melanin stacked oligomer particles' surface exposed to the high oxidative environment. When we turn to the bulk result (e.g., 600 seconds), we see some changes in carbon peaks, some in the oxygens, but in either case, not nearly as much as was observed for the pellets. It appears that the thin-film processing removed the oxygen impurity, or the pellet press for pellet sample imparted a contaminant, or the films are less conducive to adsorb pollutants from the environment. Again, the nitrogen peak shows a distinct difference, with a shift to higher energy. Furthermore, we see similar behavior for the other thin-film samples, which indicate that the solution process leads to some chemical redistribution, either by altering the π-π staking strength or changing some of the underlying chemistry of indole structure. However, to gain a deeper understanding of the chemistry involved, especially the nitrogen, we undertook the modeling of the depth profile results that are shown in Figure 3 (d-i).

The overall depth profile behavior of the thin-films modeling is in accordance with the results from the pellets, nonetheless, with some divergences. Similarly to pellet data, CxHy, C-O/C-N and C=O contributions do not suffer significant differences with etching. Still, the O-C=O varies differently, probably due to the oxidative environment caused by ammonia. Even though we have considered π-π* satellite in the simulations, their intensities were negligible compared to the other peaks. This could be related to possible oligomeric sheets' destacking effect caused by water or alkaline solution [51,53,54]. Also, it is possible to see that the change in intensity of O-C (Figure 3 (h)) and =NR (Figure 3 (i)) are smaller than what was seen in powder, which could be related to fewer impurities adsorbed in the film as mentioned before. The main difference was the presence of a broad peak at 536.0 ± 0.5 eV that can be attributed to sodium Auger electrons originated from the glass substrates [55] and the absence of the peak related to non-cyclized structures. In any case, it does appear that for the films, the surface and the bulk profiles are much closer to one another than the pellet samples. Therefore, it would

appear that thin-film characterization of the surface scan is an even better approximation of the chemical composition, demonstrating the potential for elemental composition characterization of melanin by XPS.

Synthetic Non-Functionalized Soluble Melanin Samples

In order to evaluate if the above discussion could be applied to other samples, we have considered different soluble, non-functionalized melanin derivatives and soluble sulfonated melanin derivatives (which we will turn to in a little while).

The two water-soluble non-functionalized melanin derivatives chosen to be studied here were obtained by slightly changing the synthetic parameters of each sample. These samples have similar structures to the standard one discussed above. Still, they tend to show a higher amount of carboxylic acid content or, alternatively, an increase in its oxidation state [35]. Our study begins with the estimation of the atomic content for carbon (C1s), oxygen (O1s) and nitrogen (N1s) and their ratios for the pellet and thin-film systems. However, we will first focus on the pellet morphology data, as presented in Table 3, which shows the atomic percentages and ratios after excluding the of sulfur (S2p), calcium (Ca2p) and silicon (Si2p) impurities (see Table S1).

Table 3. The atomic composition (atomic concentration %) and atomic ratios determined from pressed powder pellets of soluble non-functionalized melanin samples.

Samples	**C** (at%)	**O** (at%)	**N** (at%)	**C/N**	**O/N**	**C/O**
NF-DHI (Theoretical)	72.7	18.2	9.1	8	2	4
NF-DHICA (Theoretical)	64.3	29.6	7.1	9	4	2.2
NFMel-S (Pellet surface)	67.6	23.3	9.2	7.4	2.5	2.9
NFMel-S (Pellet bulk)	71.2	17.7	11.1	6.4	1.6	4.0
NFMel-6P (Pellet surface)	65.9	24.5	9.6	6.9	2.5	2.7
NFMel-6P (Pellet bulk)	68.4	20.2	11.4	6.0	1.8	3.4

The XPS C/O/N content of NFMel-S and NFMel-6P present in Table 3 is compatible with the one found for NFMel-I, indicating that these samples are also a combination of DHI and DHICA monomers. To deepen our analysis, we also evaluate the high-resolution depth profiling

spectra of NFMel-S and NFMel-6P and they are displayed in Figure 4(a-c, g-i).

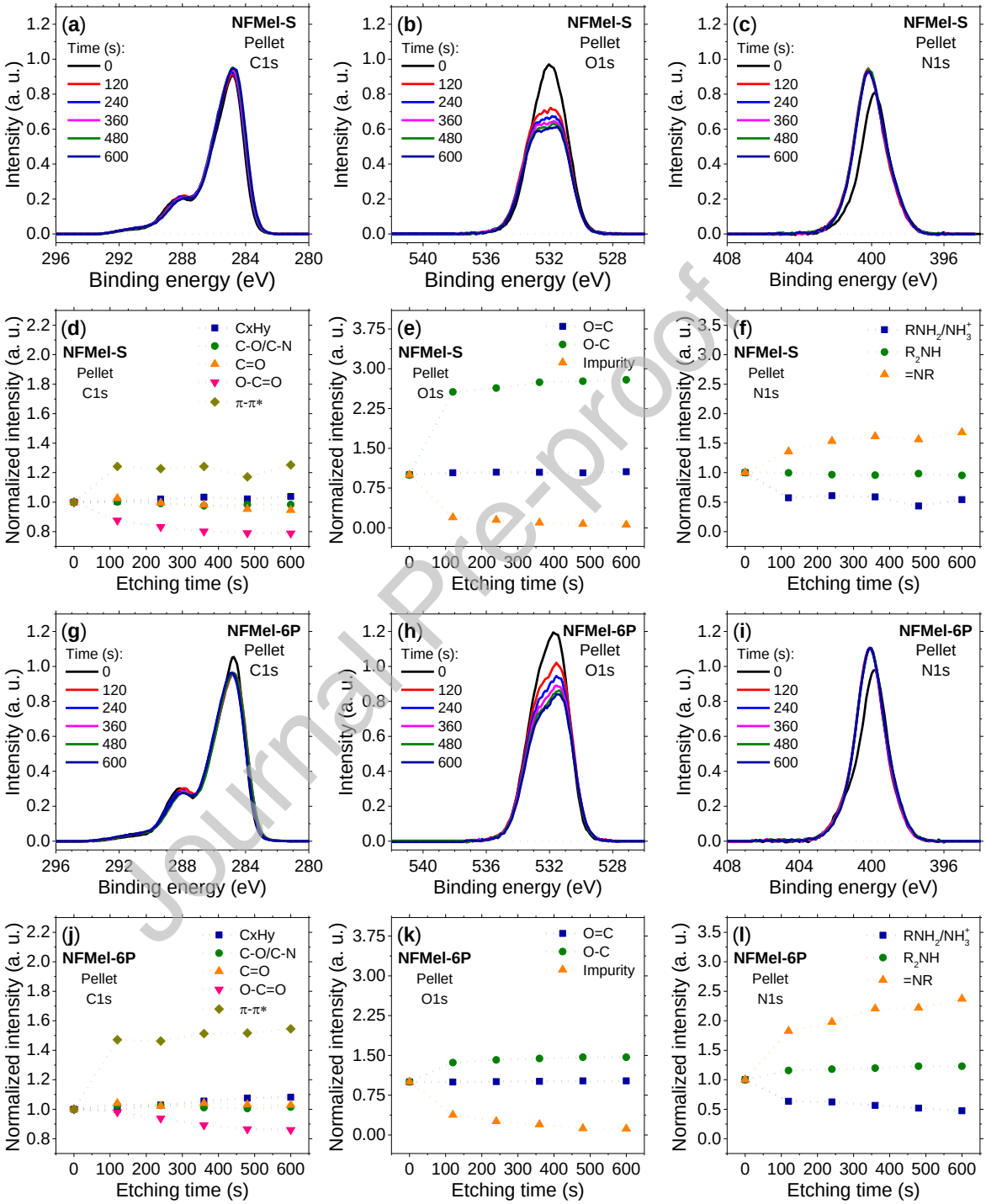

Figure 4. (a-c, g-i) C1s, O1s and N1s high-resolution XPS depth profiling for NFMel-S and NFMel-6P pellet (see legend). (d-f, j-l) XPS functional groups distribution for NFMel-S and NFMel-6P pellets as a function of etching time.

Comparing both the surface (0 s) and the bulk (600 s) of each material, in the same way we did above for NFMel-I, one can also see a decrease in the O1s spectrum area (of about 22.7% for NFMel-S and 21.9 % for NFMel-6P) and an increase in the N1s spectrum area (of 23.9 % for NFMel-S and 12.8 % for NFMel-6P) after the etching. Another feature of N1s spectra is that there is also a slight shift towards higher energy (+ 0.2 eV for NFMel-S and NFMel-6P)

The modeling analysis of these spectra was identical to the NFMel-I for all the C1s, O1s and N1s regions (Figure 2(d-f)). The only difference was the atomic composition intensity of each peak that is shown in Figure 4(d-f, j-l). The variation of each peak assignment has the same comportment of the ones in Figure 2(g-i) for NFMel-I, indicating that the different melanin samples have the same behavior with etching. Therefore, such a result implies, again, that a surface scan can be an excellent alternative to obtain the elemental composition of the system with a fine approximation to all modeling peaks for all kinds of "standard melanin".

We now tackle the thin-film morphologies of NFMel-S and NFMel-6P samples. Initially, our focus was on the atomic composition of the films prepared with water and ammonia mixtures. The results present in Table 4 show the renormalized values to exclude possible film contaminants (see in Table S3 the composition of sulfur S2p, calcium Ca2p, silicon Si2p and sodium Na1s).

Table 4. The atomic composition (atomic concentration %) and atomic ratios determined from spin-coated thin-films of soluble non-functionalized melanin samples from H_2O+NH_3 solutions.

Samples	**C** (at%)	**O** (at%)	**N** (at%)	**C/N**	**O/N**	**C/O**
NFMel-S (H_2O+NH_3 film surface)	62.3	25.2	12.5	5.0	2.0	2.5
NFMel-S (H_2O+NH_3 film bulk)	60.7	23.3	16.0	3.8	1.5	2.6
NFMel-6P (H_2O+NH_3 film surface)	57.9	29.4	12.7	4.6	2.3	2.0
NFMel-6P (H_2O+NH_3 film bulk)	56.3	27.8	15.9	3.5	1.8	2.0

Once more, the comportment we observe for the soluble samples is compatible with NFMel-I. That is, there is an increase in the nitrogen content of the film with a slight decrease in carbon and oxygen content. As we mentioned before, such variation can be related to the

remolding of the oligomer particles' surface. However, what caught the most attention was the higher variation of the atomic composition of NFMel-6P in comparison to NFMel-S (that is more or less the same as NFMel-I), which could imply that such sample is more unstable under high oxidative environment cause by the ammonia. Therefore, to evaluate the possible effect of the ammonia solution in these samples and understanding of the chemistry involved, we combine the analysis of the high-resolution spectra with their modeling, shown in Figure 5. The same number of peaks as used for NFMel-I (Figure 3(d-f)) was necessary for NFMel-S and NFMel-6P, but with differences in intensity.

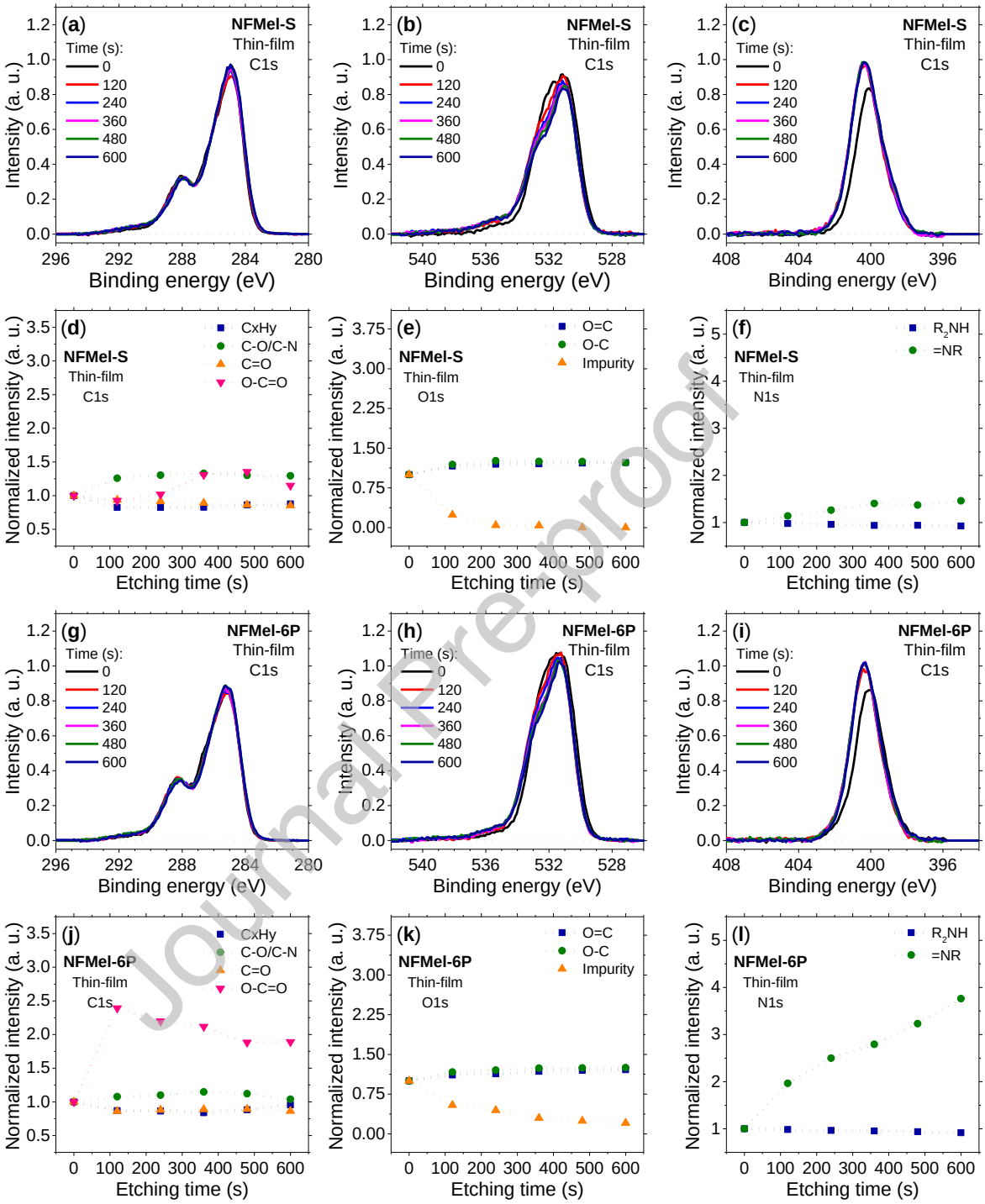

Figure 5. (a-c, g-i) C1s, O1s and N1s high-resolution XPS depth profiling for NFMel-S and NFMel-6P thin-films (see legend) following the standard water and ammonia procedure. (d-f, j-l) XPS functional groups distribution for NFMel-S and NFMel-6P thin-film from water & ammonia procedure as a function of etching time.

The result present in Figure 5 indicates that there is no significant differences between the surface and the bulk of each thin-film samples. The main differences are related to O-C=O and =NR peaks of NFMel-6P that changes with the fabrication procedure or even with etching. Such variation could be a consequence of the higher oxidation state of NFMel-6P that lead to smaller particles (compared to NFMel-S) [35] that are unable to withstand the deposition process and the etching step, or it could be related to the higher amount of oxygen impurity as we can see in Figure 5(e, k).

Now, we turn to NFMel-S and NFMel-6P thin-film prepared using only water. The atomic percentages and ratios of each sample are given in Table 5 with their resultant depth profile XPS spectra in Figure 6. Table 5 shows the renormalized data to exclude calcium (Ca2p), sulfur (S2p), silicon (Si2p) and sodium (Na1s) impurities (see Table S3).

Table 5. The atomic composition (atomic concentration %) and atomic ratios determined from spin-coated thin-films of soluble non-functionalized melanin samples from H_2O solutions.

Samples	**C** (at%)	**O** (at%)	**N** (at%)	**C/N**	**O/N**	**C/O**
NFMel-S (H_2O film surface)	64.0	25.5	10.5	6.1	2.4	2.5
NFMel-S (H_2O film bulk)	60.8	25.7	13.5	4.5	1.9	2.4
NFMel-6P (H_2O film surface)	61.1	27.9	11.0	5.5	2.5	2.2
NFMel-6P (H_2O film bulk)	60.7	26.4	12.9	4.7	2.0	2.3

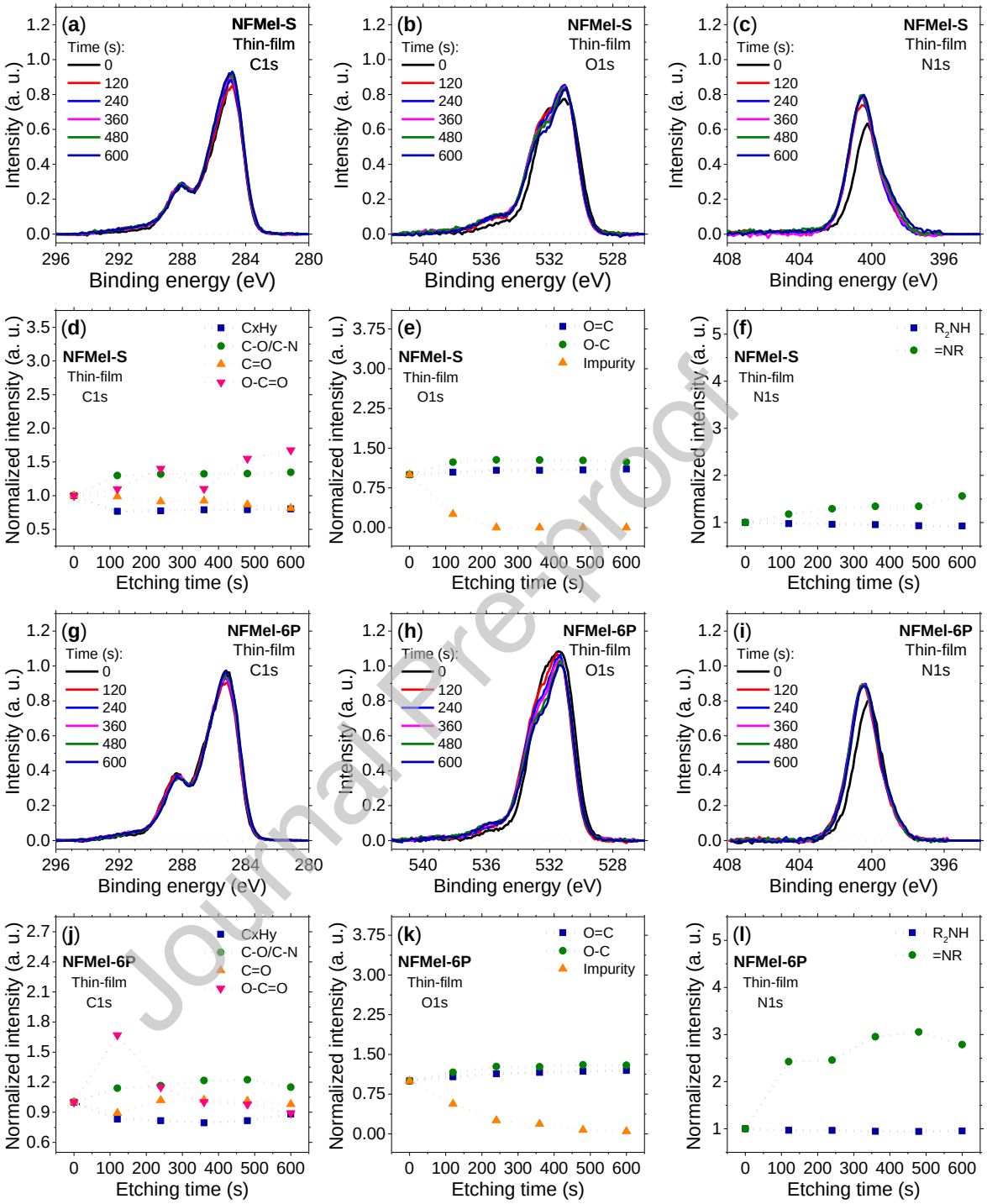

Figure 6. (a-c, g-i) C1s, O1s and N1s high-resolution XPS depth profiling for NFMel-S and NFMel-6P thin-films (see legend) using the water-only procedure. (d-f, j-l) XPS functional groups distribution for NFMel-S and NFMel-6P thin-film from water procedure as a function of etching time.

Initially, we had expected that the estimation of the elemental analysis of the H_2O thin-films would be similar to the pellets data (Table 3) because no high oxidation environment was used to prepare the films. However, comparing the data from Table 5 to Table 3 & 4, it appears that the values are within both pellet and H_2O+NH_3 thin-film results. These values may reflect simply sample to sample variation due to the chemical heterogeneity of melanins or that the overall deposition procedure is somewhat affecting the macrostructure organization of the melanin samples. In any case, the atomic values are consistent for the surface and depth profile of the bulk, corroborating that a basic surface XPS scan essentially captures the bulk elemental composition for these materials.

When it comes to the details of the underlying chemistry, the actual XPS profiles in Figure 6, when compared to previous data above (Figure 4 and Figure 5), show some differences. For instance, the intensity of the surface C1s peaks changes as we go deeper into the sample, but the differences are consistent with all the etching. Such behavior could indicate that the surface chemistry was altered or using water during deposition, the surface is more affected by the impurities, which could imply that the ammonia could assist the cleaning of the samples.

Another interesting result is that comparing the O-C=O and =NR peaks of NFMel-6P from ammonia solution (Figure 5(j, l)) with only water (Figure 6(j, l)), it is possible to observe that there is significant alteration in its intensity, implying that the ammonia and the deposition process can influence the chemistry of, at least, NFMel-6P.

In short, NFMel-S and NFMel-6P behave similarly to NFMel-I in all aspects. Therefore, these results corroborate our initial proposal that the chemical composition of both pellets and the thin-films (spun out of H_2O+NH_3 or just H_2O) surface can be a good approximation of the bulk a particular melanin sample.

Powdered Synthetic Sulfonated Melanin Samples

We now turn our attention to the investigation of other synthetic melanin systems that has a more complex structure to see whether the trends observed above continue. The data presented below are on sulfonated melanin that incorporates sulfonated structures (Figure 1(b)) in the basic DHI and DHICA monomer moieties. It is necessary to stress that, in addition to the presence of sulfonated groups, these samples have slightly different oxidation (SMel-T < SMel < SMel-8P < SMel-4P) states and polymerization structures through carbon (SMel and SMel-T) or oxygen (SMel-4P and SMel-8P) bonds [34,36].

The C1s, O1s, N1s, and S2p atomic ratios were obtained for the sulfonated samples and are shown in Table 6. Note that such values do not take into account calcium (Ca2p) and silicon (Si2p) impurities (see Table S4). For comparison, we also show the theoretical values expected for sulfonated-DHI (S-DHI) and sulfonated-DHICA (S-DHICA) monomers considering the presence of only one sulfonated group attached in any of the possible positions (Figure 1(b)).

Table 6. The atomic composition (atomic concentration %) and atomic ratios determined from pressed powder pellets of sulfonated melanin samples.

Samples	**C** (at%)	**O** (at%)	**N** (at%)	**S** (at%)	**C/N**	**O/N**	**S/N**	**C/O**
S-DHI (Theoretical)	60.1	26.7	6.7	6.7	9	4	1	2.25
S-DHICA (Theoretical)	55.6	33.3	5.6	5.6	10	6	1	1.7
SMel (Pellet surface)	72.3	22.4	3.5	1.8	20.7	6.4	0.5	3.2
SMel (Pellet bulk)	76.1	17.9	4.3	1.7	17.6	4.2	0.4	4.2
SMel-T (Pellet surface)	69.6	23.2	4.4	2.8	15.9	5.3	0.6	3.0
SMel-T (Pellet bulk)	75.4	16.9	5.2	2.5	14.4	3.2	0.5	4.5
SMel-4P (Pellet surface)	66.1	25.0	5.6	3.4	11.8	4.5	0.6	2.6
SMel-4P (Pellet bulk)	69.7	20.1	7.0	3.2	9.9	2.9	0.5	3.5
SMel-8P (Pellet surface)	67.0	24.1	5.8	3.0	11.5	4.1	0.5	2.8
SMel-8P (Pellet bulk)	70.1	20.1	6.8	2.9	10.3	2.9	0.4	3.5

Based on the elemental analysis shown in Table 6, one may see that the C/O/N/S amount is different from the theoretical considering the proposed sulfonated structure. However, they are compatible with the non-functionalized monomers (see Table 1 to Table 3), which suggests that not all monomer moieties have sulfonated groups attached to them as confirmed by the ~0.5 atomic ratio of S/N. What also catches the attention was the low amount of nitrogen for SMel and SMel-T, which is probably related to the chemical heterogeneity discussed in the introduction section. However, we cannot completely rule out the possibility that other chemical entities have replaced some of the nitrogen from DL-DOPA before intramolecular cyclization or

that the sulfur group could potentially de-stabilize the DL-DOPA nitrogen and remove it from the melanin precursor. In-depth analysis with ^{15}N, ^{33}S and ^{1}H-^{13}C nuclear magnetic resonance technique should assist a more precise structural elucidation; however, they are not in the scope of the present study.

As we aim to evaluate if the surface analysis of the sulfonated melanin samples is a good representation of the bulk, we also inspected the depth profile of these samples. Figure 7 shows the C1s, O1s, N1s, and S2p spectra for SMel pellets. The same behavior was found for the other three samples, and their spectra are shown in Figure S2-S4.

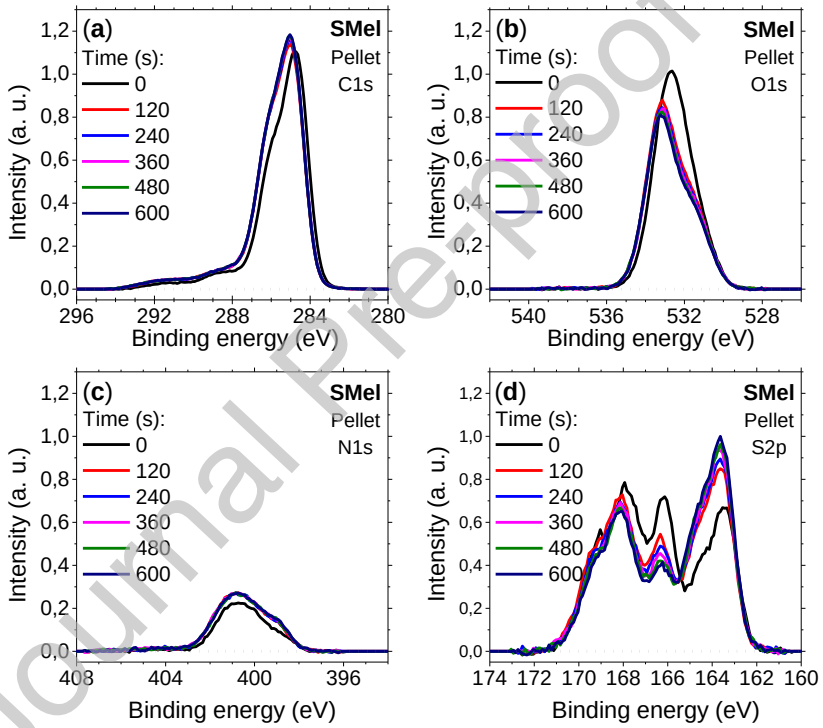

Figure 7. C1s, O1s, N1s and S2p high-resolution XPS depth profiling of SMel pellet.

By comparing Figure 7 with the non-functionalized melanin pellet spectra in Figure 2 and Figure 4, it is possible to observe that the overall high-resolution depth profile behaves in the same manner with a decrease in the O1s spectrum area of 15.3 % and an increase of 31.8 % for N1s. The main differences are related to a higher intensity of S2p spectra (with 1.4% variation between surface and bulk) and the slight increase (about 11.3 %) of the C1s spectrum area, which can be attributed to the sulfonated groups attached to the melanin indole ring. Another divergence is the absence of a significant shift of the N1s peak position with etching, in

agreement with an earlier preposition that sulfonated melanin has a less densely packed structure [36].

Here, we also investigate the chemistry involved in this sample using depth-profile modeling, see Figure 8. The assigned chemical groups with their respective energies are listed in Table S6. Again, in this case, the same model was applied to the other sulfonated samples and the result are shown in Figure S5.

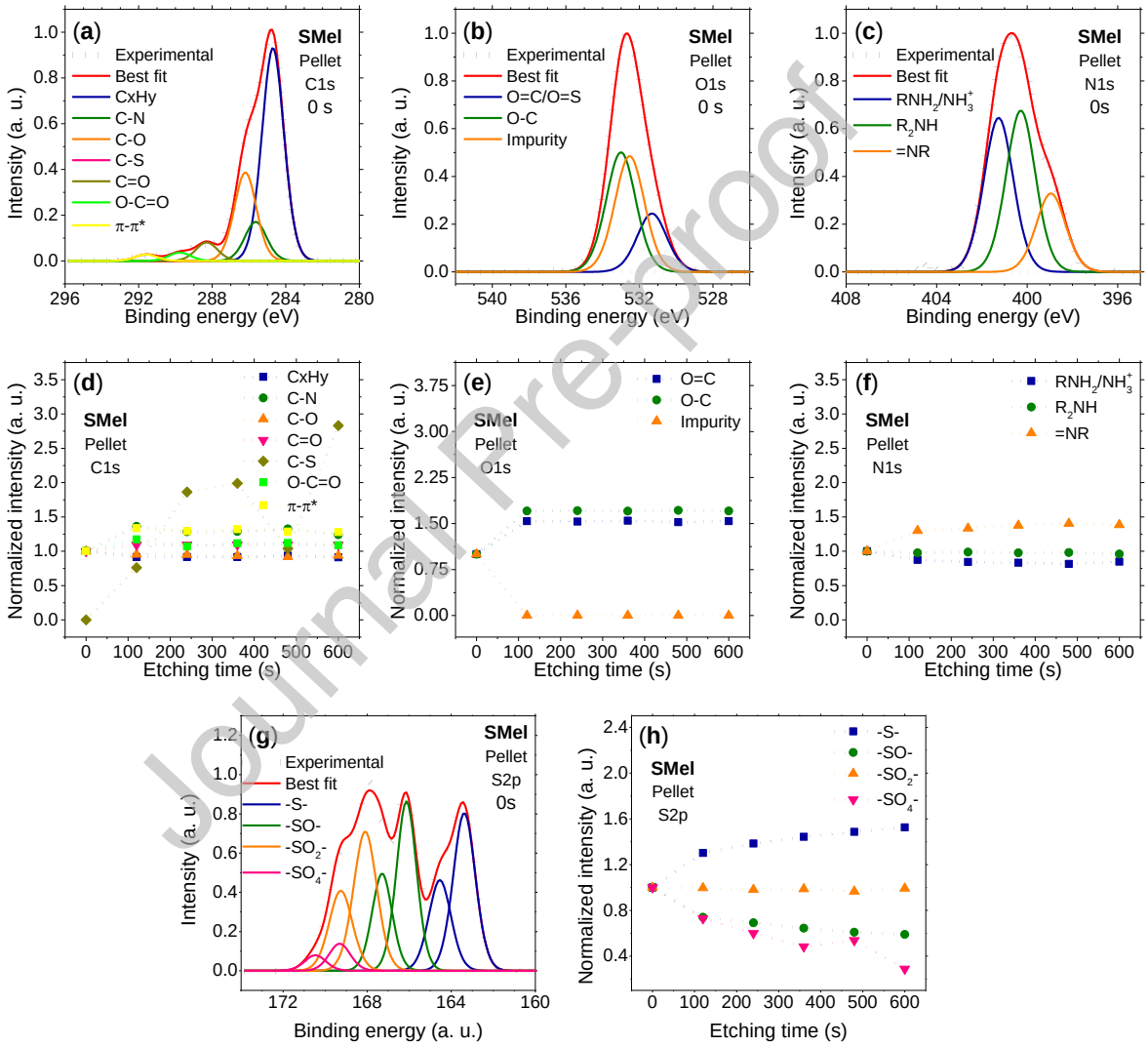

Figure 8. (a, b, c, g) C1s, O1s, N1s and S2p high-resolution XPS spectra simulation for the SMel pellet surface. The same modeling was applied to the depth profile spectra. For S2p high-resolution spectra, high intensity and low binding energy refer to S2p3/2, whereas the opposite to S2p1/2. (d, e, f, h) Functional group distribution as a function of etching time normalized by the surface intensity.

For sulfonated melanin, seven carbon species (CxHy, C-N, C-O, C-S C=O, O-C=O and π-π*) were considered to fit the C1s region. As shown in Figure 8(b), the peaks attributed to the basic melanin structure do not vary with etching, indicating that the same structure is obtained for both surface and bulk. The only variation was related to the C-S peak that can be associated with the sulfonated groups and to DMSO trapped in between melanin layers. In the same way, the oxygen peak was deconvoluted to three components related to O-C and O=C/O=S bonds from ketones, hydroxyl, carboxyl and sulfonated groups and oxygen impurities absorbed at the surface. N1s region was fitted considered three different nitrogen species: R_2-NH as the main specie related to indole structure, =NR related to imine group and RNH_2/NH_3^+ from non-cyclized forms. The proposed model is compatible with non-functionalized melanin, which could point to similar systems.

Additionally, note that both O1s and N1s also do not suffer significant variations with etching, indicating high stability of the sulfonated melanin macrostructure. The S2p spectrum shows three significant contributions from -S-, -SO- and -SO_2- that are associated with the sulfonated groups and synthetic DMSO, whereas another component of low intensity and high binding energy was ascribed to -SO_4- from synthetic by-product contamination [36]. Such behavior is corroborated by the atomic ratio evolution of each contribution normalized by the nitrogen' atomic concentration (see Table S5). Figure 8(h) indicates that there is not a high deviation between surface and bulk of sulfonated melanin, of which the small variations could be understood with the removal of synthetic impurities in the samples. Therefore, the result present here agrees with our previous discussion that we can use a surface analysis also to characterize the bulk of sulfonated melanin derivative.

Thin Film Synthetic Sulfonated Melanin Samples

Thin-films of SMel are usually made from DMSO solution [9,14,18,37,38,56,57]; however, recently, it has been shown that sulfonated melanin samples are also soluble in solvents like DMF and NMP [36]. Thus, we intend to evaluate the interaction of each derivative with these different solvents and verify if the surface of the thin-film is still compatible with its bulk. Hence, Table 7 presents the elemental analysis obtained at the surface of each film and Figure 9 of their depth profile. In the present case, Table 7 also exclude the impurities of calcium (Ca2p), silicon (Si2p) and sodium (Na1s), see Table S6.

Table 7. The atomic composition (atomic concentration %) and atomic ratios determined from the surface of spin-coated thin films of sulfonated melanin samples.

Samples	Solvents	C (at%)	O (at%)	N (at%)	S (at%)	C/N	O/N	S/N	C/O
S-DHI (Theoretical)	#	60.1	26.7	6.7	6.7	9	4	1	2.25
S-DHICA (Theoretical)	#	55.6	33.3	5.6	5.6	10	6	1	1.7
SMel	DMSO	66.1	29.4	3.3	1.1	19.9	8.8	0.3	2.2
	DMF	74.1	22.1	2.9	0.9	25.2	7.5	0.3	3.4
	NMP	61.5	34.0	3.5	1.1	17.6	9.7	0.3	1.8
SMel-T	DMSO	64.7	29.9	3.9	1.6	16.7	7.7	0.4	2.2
	DMF	67.0	26.8	4.3	1.9	15.5	6.2	0.4	2.5
	NMP	60.4	33.4	4.6	1.7	13.2	7.3	0.4	1.8
SMel-4P	DMSO	56.4	34.8	6.9	1.8	8.2	5.0	0.3	1.6
	DMF	66.5	27.3	4.5	1.7	14.8	6.1	0.4	2.4
	NMP	56.5	36.1	5.6	1.8	10.2	6.5	0.3	1.6
SMel-8P	DMSO	57.4	35.1	6.4	1.0	9.0	5.5	0.2	1.6
	DMF	67.7	26.3	4.4	1.6	15.4	6.0	0.4	2.6
	NMP	58.1	33.9	6.1	1.9	9.5	5.5	0.3	1.7

The values displayed in Table 7 and Table S7 are in agreement with the pellet analysis (Table 6), indicating that pieces of information about the basic melanin structure, i.e., aromatic carbon structure, is not lost, as evidenced by the C1s, O1s, and N1s high-resolution spectra in Figure 9. However, S2p spectra do show small changes. Such variations can not necessarily be related to a fundamental alteration in the melanin structure; instead, it could only be a response of higher concentration of the solvent trapped in between the melanin particles or to some modifications in the sulfonated group due to instability of this group [28]. In fact, when analyzing the chemistry information of the sample, evidenced in Table 8 (without calcium

(Ca2p), silicon (Si2p) and sodium (Na1s) impurities, see Table S8.), Figure 10 and Figures S6-S8, we cannot see higher variations when comparing the surface and the bulk. The more considerable variation observed with NMP solution (Figure 9, Figure 10 and Figures S2-S8) that could only be an indication that the films are not thick enough or are not homogeneous so that the glass substrate is contributing to the signal, as evidenced by the higher proportion of impurities in Table S8. Additionally, note that the thin-films fabrication process of sulfonated melanin also shows the ability to be able to clean the sample, as there was no need to use the peak assigned to synthesis impurities (-SO_4-) to fit the S2p high-resolution spectra.

Table 8. The atomic composition (atomic concentration %) and atomic ratios determined from the bulk of spin coated thin films of sulfonated melanin samples.

Samples	**Solvents**	**C** (at%)	**O** (at%)	**N** (at%)	**S** (at%)	**C/N**	**O/N**	**S/N**	**C/O**
S-DHI (Theoretical)	#	60.1	26.7	6.7	6.7	9	4	1	2.25
S-DHICA (Theoretical)	#	55.6	33.3	5.6	5.6	10	6	1	1.7
SMel	DMSO	67.8	27.1	4.2	0.9	16.3	6.5	0.2	2.5
	DMF	72.4	22.4	4.3	1.0	17.0	5.2	0.2	3.2
	NMP	8.4	90.9	0.6	0.2	13.5	147.2	0.3	0.1
SMel-T	DMSO	58.0	35.8	4.6	1.6	12.5	7.7	0.3	1.6
	DMF	71.3	21.4	5.4	1.9	13.1	3.9	0.3	3.3
	NMP	62.7	30.3	5.4	1.6	11.7	5.6	0.3	2.1
SMel-4P	DMSO	53.0	38.0	7.5	1.6	7.1	5.1	0.2	1.4
	DMF	74.4	18.9	5.0	1.7	14.7	3.7	0.3	3.9
	NMP	7.5	90.8	1.2	0.4	6.3	75.7	0.3	0.1
SMel-8P	DMSO	55.7	36.5	6.9	0.9	8.1	5.3	0.1	1.5
	DMF	71.3	22.1	4.8	14.7	4.6	4.6	0.4	3.2
	NMP	12.5	85.8	1.6	0.1	7.9	54.3	0.1	0.1

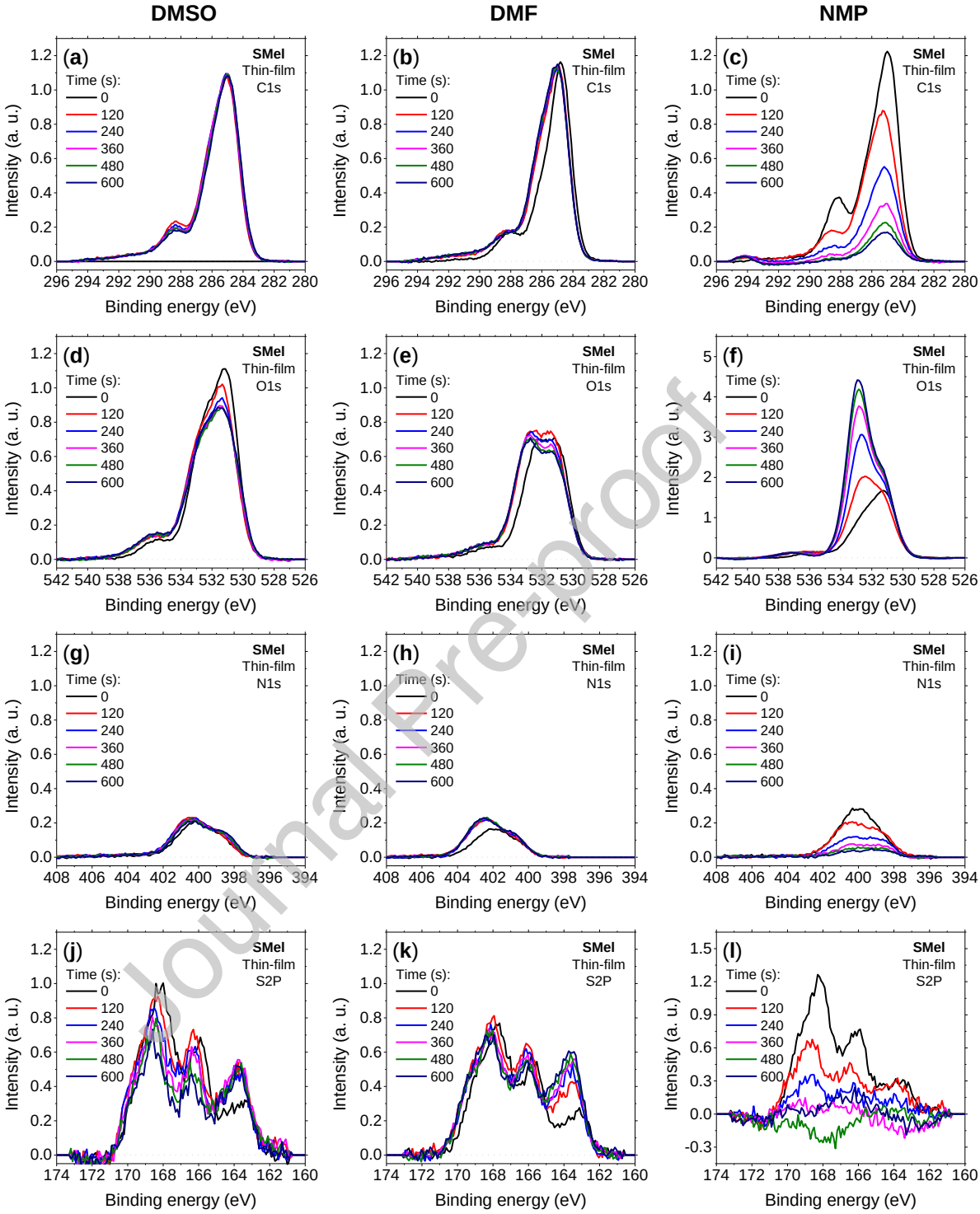

Figure 9. High-resolution (a-c) C1s, (d-f) O1s, (g-i) N1s, and (j-l) S2p XPS depth profiling of SMel thin-film from DMSO (left column), DMF (middle column) and NMP (right column) solutions.

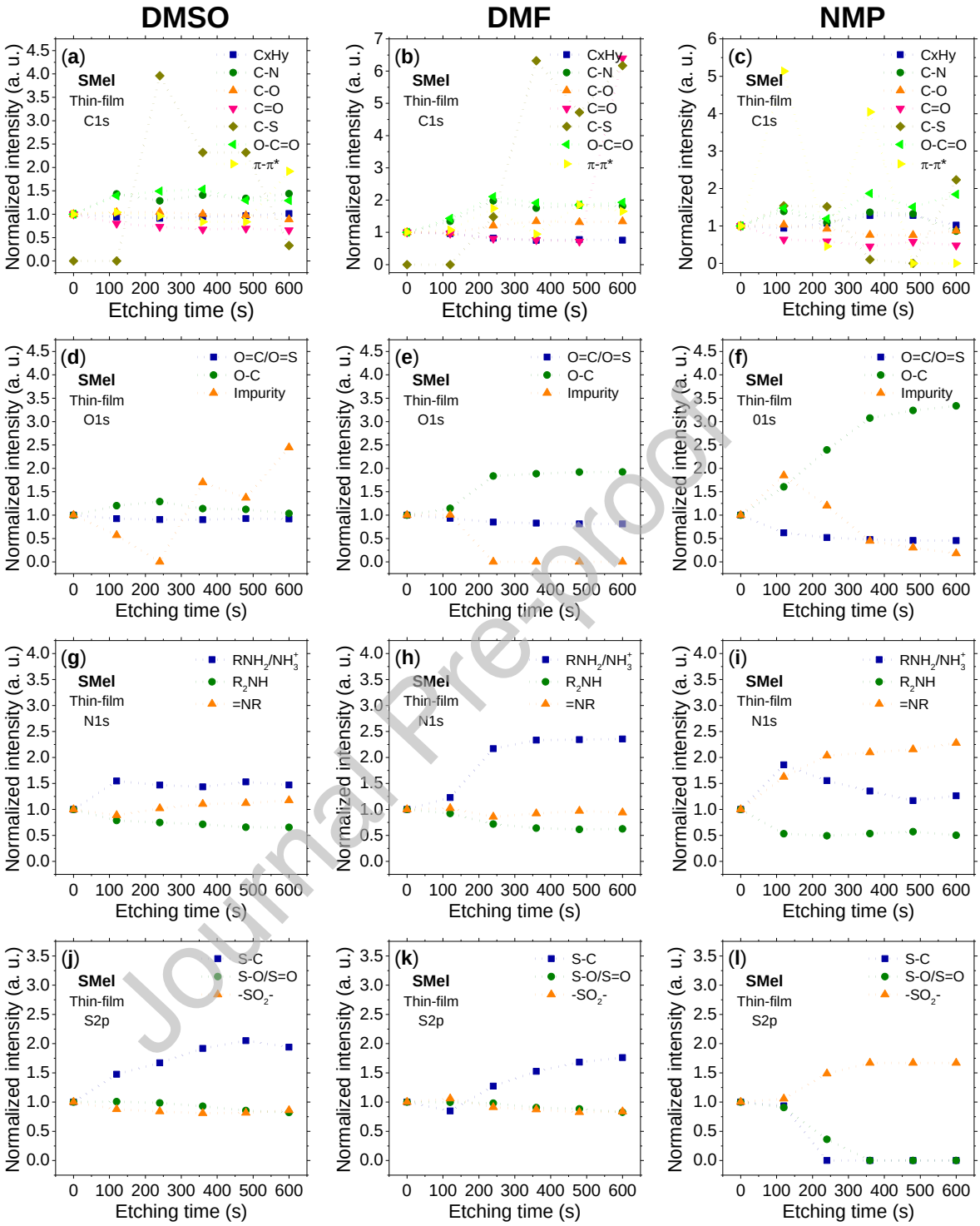

Figure 10. XPS functional groups distribution for SMel thin-film from DMSO (left column), DMF (middle column), and NMP (right column) solutions as a function of etching time. The surface intensity normalized the intensity of each group.

Therefore, based on what we have shown in this section, we have demonstrated that the

film deposition process, regardless of which solvent is used, does not change the basic structure of melanin. In addition, no very significant variation was observed when comparing the surface and bulk of the sample, corroborating our proposal.

In regards to potential polyindolequione systems containing metal ions, a recent study [8] in which Cu(II) was incorporated into a melanin sample showed that one can obtain qualitative insight into the chemistry, but no real quantitative atomic ratio analysis due overlapping from oxygen species higher energy peaks. Hence, any future study of systems with metal ions will require a case by case assessment.

To conclude, in light of the above observations, we presented evidences towards the use of surface XPS scan to obtain the elemental composition of any melanin or polyindolequione derivative with non-metallic atoms because the surface seems to be a good representation of the bulk structure.

Conclusions

From the work presented here, there are a couple of basic rules that can be applied to the study of melanins, or polyindolequinone in general, including the polydopamines, that do not include metallic atoms. The first is that a surface scan of any polyindolequinone system (no matter the morphology) will essentially give the same atomic ratio as the bulk and, therefore, XPS is an excellent tool for elemental analysis. The second rule is that, for standard melanins, there are slight differences in the chemistry of the bulk and the surface. The final rule is for standard melanin thin-films and all morphologies of the other melanins (soluble and sulfonated), the atomic chemistry of the surface is representative of the bulk as well. This is good news for work on technological applications for these systems, which rely on thin-film morphologies. Using XPS surface scans to obtain chemistry of the bulk will greatly expedite research efforts on the poly indolequinone systems.

Overall, the data shows that the use of XPS as an elemental analysis tool has been placed on a firmer footing and should be part of the basic characterization of the polyindolequinone systems.

Author Statement

Dear Dr. Chipara,

Please see attached our re-worked manuscript entitled "*Melanin system composition analyzed by XPS depth profiling*". We wish to thank you and the reviewers for their comments.

A detailed description of our response and changes to the manuscript are presented below. We believe that we have adequately responded to all comments and we anticipate that you yourself will agree that the work is ready for publication.

In making this resubmission, I affirm that all authors have made significant contributions to the research and have read and approved the final version.

Declaration of interests

The authors declare that they have no known competing financial interests or personal relationships that could have appeared to influence the work reported in this paper.

The authors declare the following financial interests/personal relationships which may be considered as potential competing interests.

Acknowledgment

JVP and CFOG gratefully acknowledge the financial supports of São Paulo Research Foundation (FAPESP; grants 2013/07296-2, 2015/23000-1, 2018/02411-1). A.B.M. is a Sêr Cymru II fellow and the results incorporated in this work have received funding from the European Union's Horizon 2020 research and innovation program under the Marie Skłodowska-Curie grant agreement No 663830. J.D.McG thank the EPSRC SPECIFIC project for funding (EP/N020863/1) & WEFO (ERDF) project AIM (80708 & EP/M015254/2) for their ongoing support for XPS maintenance. We thank Prof. Paul Meredith for his thoughts.

References

[1] P. Meredith, T. Sarna, The physical and chemical properties of eumelanin., Pigment Cell Res. 19 (2006) 572–94. https://doi.org/10.1111/j.1600-0749.2006.00345.x.

[2] G. Prota, Melanins and melanogenesis, Academic Press, 1992.

[3] J.Y. Lin, D.E. Fisher, Melanocyte biology and skin pigmentation., Nature. 445 (2007) 843–50. https://doi.org/10.1038/nature05660.

[4] F.A. Zucca, G. Giaveri, M. Gallorini, A. Albertini, M. Toscani, G. Pezzoli, R. Lucius, H. Wilms, D. Sulzer, S. Ito, K. Wakamatsu, L. Zecca, The neuromelanin of human substantia nigra: Physiological and pathogenic aspects, Pigment Cell Res. 17 (2004) 610–617. https://doi.org/10.1111/j.1600-0749.2004.00201.x.

[5] N. Amdursky, E.D. Głowacki, P. Meredith, Macroscale Biomolecular Electronics and Ionics, Adv. Mater. 31 (2019) 1802221. https://doi.org/10.1002/adma.201802221.

[6] P. Meredith, B.J. Powell, J. Riesz, S.P. Nighswander-Rempel, M.R. Pederson, E.G. Moore, Towards structure–property–function relationships for eumelanin, Soft Matter. 2 (2006) 37–44. https://doi.org/10.1039/b511922g.

[7] L. Hong, J.D. Simon, Current understanding of the binding sites, capacity, affinity and biological significance of metals in melanin, J. Phys. Chem. B. 111 (2007) 7938–7947. https://doi.org/10.1021/jp071439h.

[8] A.B. Mostert, S. Rienecker, M. Sheliakina, P. Zierep, G.R. Hanson, J.R. Harmer, G. Schenk, P. Meredith, Engineering Proton Conductivity in Melanin Using Metal Doping, J. Mater. Chem. B. 8 (2020) 8050–8060. https://doi.org/10.1039/d0tb01390k.

[9] S.N. Dezidério, C.A. Brunello, M.I.N. da Silva, M.A. Cotta, C.F.O. Graeff, Thin films of synthetic melanin, J. Non. Cryst. Solids. 338–340 (2004) 634–638. https://doi.org/10.1016/j.jnoncrysol.2004.03.058.

[10] H. Lee, S.M. Dellatore, W.M. Miller, P.B. Messersmith, Mussel-inspired surface chemistry for multifunctional coatings, Science (80-.). 318 (2007) 426–430. https://doi.org/10.1126/science.1147241.

[11] J.P. Bothma, J. de Boor, U. Divakar, P.E. Schwenn, P. Meredith, Device-Quality Electrically Conducting Melanin Thin Films, Adv. Mater. 20 (2008) 3539–3542. https://doi.org/10.1002/adma.200703141.

[12] M. Abbas, F. D'Amico, L. Morresi, N. Pinto, M. Ficcadenti, R. Natali, L. Ottaviano, M. Passacantando, M. Cuccioloni, M. Angeletti, R. Gunnella, Structural, electrical, electronic and optical properties of melanin films, Eur. Phys. J. E. 28 (2009) 285–291. https://doi.org/10.1140/epje/i2008-10437-9.

[13] M. Ambrico, P.F. Ambrico, A. Cardone, T. Ligonzo, S.R. Cicco, R. Di Mundo, V. Augelli, G.M. Farinola, Melanin layer on silicon: An attractive structure for a possible exploitation in bio-polymer based metal-insulator-silicon devices, Adv. Mater. 23 (2011) 3332–3336. https://doi.org/10.1002/adma.201101358.

[14] J. Wünsche, F. Cicoira, C.F.O. Graeff, C. Santato, Eumelanin thin films: solution-processing, growth, and charge transport properties, Jounal Mater. Chem. B. 1 (2013) 3836–3842. https://doi.org/10.1039/c3tb20630k.

[15] M. Piacenti-Silva, J.C. Fernandes, N.B. de Figueiredo, M. Congiu, M. Mulato, C.F. de O. Graeff, Melanin as an active layer in biosensors, AIP Adv. 4 (2014) 037120-1/037120-8. https://doi.org/10.1063/1.4869638.

[16] A.J. Clulow, A.B. Mostert, M. Sheliakina, A. Nelson, N. Booth, P.L. Burn, I.R. Gentle, P. Meredith, The structural impact of water sorption on device-quality melanin thin films, Soft Matter. 13 (2017) 3954–3965. https://doi.org/10.1039/c6sm02420c.

[17] L.G.S. Albano, J.V. Paulin, L.D. Trino, S.L. Fernandes, C.F. de O. Graeff, Ultraviolet-protective thin film based on PVA–melanin/rod-coated silver nanowires and its application as a transparent capacitor, J. Appl. Polym. Sci. 136 (2019) 47805. https://doi.org/10.1002/app.47805.

[18] Z. Tehrani, S.P. Whelan, B. Mostert, J.V. Paulin, M.M. Ali, E.D. Ahmadi, C.F. de O. Graeff, O.J. Guy, D.T. Gethin, Printable and Flexible Graphene pH sensors utilising Thin Film Melanin for Physiological Applications, 2D Mater. 7 (2020) 024008. https://doi.org/10.1088/2053-1583/ab72d5.

[19] M.R. Powell, B. Rosenberg, The nature of the charge carriers in solvated biomacromolecules, Bioenergetics. 1 (1970) 493–509.

https://doi.org/10.1007/BF01517187.

[20] B. Mostert, B.J. Powell, I.R. Gentle, P. Meredith, On the origin of electrical conductivity in the bio-electronic material melanin, Appl. Phys. Lett. 100 (2012) 093701. https://doi.org/10.1063/1.3688491.

[21] A.B. Mostert, B.J. Powell, F.L. Pratt, G.R. Hanson, T. Sarna, I.R. Gentle, P. Meredith, Role of semiconductivity and ion transport in the electrical conduction of melanin., Proc. Natl. Acad. Sci. U. S. A. 109 (2012) 8943–7. https://doi.org/10.1073/pnas.1119948109.

[22] J. Wünsche, Y. Deng, P. Kumar, E. Di Mauro, E. Josberger, J. Sayago, A. Pezzella, F. Soavi, F. Cicoira, M. Rolandi, C. Santato, Protonic and Electronic Transport in Hydrated Thin Films of the Pigment Eumelanin, Chem. Mater. 27 (2015) 436–442. https://doi.org/10.1021/cm502939r.

[23] S.B. Rienecker, A.B. Mostert, G. Schenk, G.R. Hanson, P. Meredith, Heavy Water as a Probe of the Free Radical Nature and Electrical Conductivity of Melanin, J. Phys. Chem. B. 119 (2015) 14994–15000. https://doi.org/10.1021/acs.jpcb.5b08970.

[24] P. Kumar, E. Di Mauro, S. Zhang, A. Pezzella, F. Soavi, C. Santato, F. Cicoira, Melanin-based flexible supercapacitors, J. Mater. Chem. C. 4 (2016) 9516–9525. https://doi.org/10.1039/c6tc03739a.

[25] M. Sheliakina, A.B. Mostert, P. Meredith, Decoupling Ionic and Electronic Currents in Melanin, Adv. Funct. Mater. 1805514 (2018) 1805514. https://doi.org/10.1002/adfm.201805514.

[26] M. Reali, P. Saini, C. Santato, Electronic and protonic transport in bio-sourced materials: a new perspective on semiconductivity, Mater. Adv. (2021) Advance Article. https://doi.org/10.1039/d0ma00579g.

[27] K.A. Motovilov, V. Grinenko, M. Savinov, Z. V. Gagkaeva, L.S. Kadyrov, A.A. Pronin, Z. V. Bedran, E.S. Zhukova, A.B. Mostert, B.P. Gorshunov, Redox chemistry in the pigment eumelanin as a function of temperature using broadband dielectric spectroscopy, RSC Adv. 9 (2019) 3857–3867. https://doi.org/10.1039/c8ra09093a.

[28] E.S. Bronze-Uhle, A. Batagin-Neto, P.H.P. Xavier, N.I. Fernandes, C.F.O. Graeff, Synthesis and characterization of melanin in DMSO, J. Mol. Struct. 1047 (2013) 102–108. https://doi.org/10.1016/j.molstruc.2013.04.061.

[29] M.B. Clark, J.A. Gardella, T.M. Schultz, D.G. Patil, L. Salvati, Solid-state analysis of eumelanin biopolymers by electron spectroscopy for chemical analysis, Anal. Chem. 62 (1990) 949–956. https://doi.org/10.1021/ac00208a011.

[30] L. Hong, J.D. Simon, Physical and chemical characterization of iris and choroid melanosomes isolated from newborn and mature cows, Photochem. Photobiol. 81 (2005) 517–523. https://doi.org/10.1111/j.1751-1097.2005.tb00219.x.

[31] F. Bernsmann, A. Ponche, C. Ringwald, J. Hemmerle, J. Raya, B. Bechinger, J.C. Voegel, P. Schaaf, V. Ball, Characterization of dopamine-melanin growth on silicon oxide, J. Phys. Chem. C. 113 (2009) 8234–8242. https://doi.org/10.1021/jp901188h.

[32] R.A. Zangmeister, T.A. Morris, M.J. Tarlov, Characterization of polydopamine thin films deposited at short times by autoxidation of dopamine, Langmuir. 29 (2013) 8619–8628. https://doi.org/10.1021/la400587j.

[33] A.B. Mostert, K.J.P. Davy, J.L. Ruggles, B.J. Powell, I.R. Gentle, P. Meredith, Gaseous adsorption in melanins: Hydrophilic biomacromolecules with high electrical conductivities, Langmuir. 26 (2010) 412–416. https://doi.org/10.1021/la901290f.

[34] M. Piacenti-Silva, E.S. Bronze-Uhle, J.V. Paulin, C.F.O. Graeff, Temperature-enhanced synthesis of DMSO-Melanin, J. Mol. Struct. 1056–1057 (2014) 135–140. https://doi.org/10.1016/j.molstruc.2013.10.041.

[35] E.S. Bronze-Uhle, J.V. Paulin, M. Piacenti-Silva, C. Battocchio, M.L.M. Rocco, C.F. de O. Graeff, Melanin synthesis under oxygen pressure, Polym. Int. 65 (2016) 1339–1346. https://doi.org/10.1002/pi.5185.

[36] J.V. Paulin, A.G. Veiga, Y. Garcia-Basabe, M.L.M. Rocco, C.F. Graeff, Structural and optical properties of soluble melanin analogues with enhanced photoluminescence quantum efficiency, Polym. Int. 67 (2018) 550–556. https://doi.org/10.1002/pi.5543.

[37] M. Piacenti-Silva, A.A. Matos, J.V. Paulin, R.A. da S. Alavarce, R.C. de Oliveira, C.F. Graeff, Biocompatibility investigations of synthetic melanin and melanin analogue for application in bioelectronics, Polym. Int. 65 (2016) 1347–1354. https://doi.org/10.1002/pi.5192.

[38] L.G.S. Albano, E. Di Mauro, P. Kumar, F. Cicoira, C.F.O. Graeff, C. Santato, Novel insights on the physicochemical properties of eumelanins and their DMSO derivatives, Polym. Int. 65 (2016) 1315–1322. https://doi.org/10.1002/pi.5167.

[39] J. V. Paulin, A. Batagin-Neto, P. Meredith, C.F.O. Graeff, A.B. Mostert, Shedding Light on the Free Radical Nature of Sulfonated Melanins, J. Phys. Chem. B. 124 (2020) 10365–10373. https://doi.org/10.1021/acs.jpcb.0c08097.

[40] C.C. Felix, J.S. Hyde, T. Sarna, R.C. Sealy, Interactions of melanin with metal ions. Electron spin resonance evidence for chelate complexes of metal ions with free radicals, J. Am. Chem. Soc. 100 (1978) 3922–3926. https://doi.org/10.1021/ja00480a044.

[41] M. D'Ischia, K. Wakamatsu, A. Napolitano, S. Briganti, J.-C. Garcia-Borron, D. Kovacs, P. Meredith, A. Pezzella, M. Picardo, T. Sarna, J.D. Simon, S. Ito, Melanins and melanogenesis: methods, standards, protocols., Pigment Cell Melanoma Res. 26 (2013) 616–633. https://doi.org/10.1111/pcmr.12121.

[42] M. V. Ivanov, T. V. Perevalov, V.S. Aliev, V.A. Gritsenko, V. V. Kaichev, Electronic structure of δ-Ta2O5 with oxygen vacancy: Ab initio calculations and comparison with experiment, J. Appl. Phys. 110 (2011) 024115. https://doi.org/10.1063/1.3606416.

[43] C.D. Wagner, D.A. Zatko, R.H. Raymond, Use of the Oxygen KLL Auger Lines in Identification of Surface Chemical States by Electron Spectroscopy for Chemical Analysis, Anal. Chem. 52 (1980) 1445–1451. https://doi.org/10.1021/ac50059a017.

[44] M. Lundholm, H. Siegbahn, S. Holmberg, M. Arbman, Core electron spectroscopy of water solutions, J. Electron Spectros. Relat. Phenomena. 40 (1986) 163–180. https://doi.org/10.1016/0368-2048(86)80015-9.

[45] G.S. Herman, Z. Dohnálek, N. Ruzycki, U. Diebold, Experimental investigation of the interaction of water and methanol with anatase-TiO2(101), J. Phys. Chem. B. 107 (2003) 2788–2795. https://doi.org/10.1021/jp0275544.

[46] S.J. Kerber, J.J. Bruckner, K. Wozniak, S. Seal, S. Hardcastle, T.L. Barr, The nature of

hydrogen in x- ray photoelectron spectroscopy: General patterns from hydroxides to hydrogen bonding, J. Vac. Sci. Technol. A Vacuum, Surfaces, Film. 14 (1996) 1314–1320. https://doi.org/10.1116/1.579947.

[47] C. V. Ramana, V. V. Atuchin, U. Becker, R.C. Ewing, L.I. Isaenko, O.Y. Khyzhun, A.A. Merkulov, L.D. Pokrovsky, A.K. Sinelnichenko, S.A. Zhurkov, Low-energy Ar- ion-beam-induced amorphization and chemical modification of potassium titanyl arsenate (001) crystal surfaces, J. Phys. Chem. C. 111 (2007) 2702–2708. https://doi.org/10.1021/jp0671392.

[48] V. V. Atuchin, L.D. Pokrovsky, O.Y. Khyzhun, A.K. Sinelnichenko, C. V. Ramana, Surface crystallography and electronic structure of potassium yttrium tungstate, J. Appl. Phys. 104 (2008) 033518. https://doi.org/10.1063/1.2963957.

[49] L.I. Isaenko, K.E. Korzhneva, S. V. Goryainov, A.A. Goloshumova, L.A. Sheludyakova, V.L. Bekenev, O.Y. Khyzhun, Structural, optical and electronic properties of K2Ba(NO3)4 crystal, Phys. B Condens. Matter. 531 (2018) 149–158. https://doi.org/10.1016/j.physb.2017.12.035.

[50] K.E. Korzhneva, V.L. Bekenev, O.Y. Khyzhun, A.A. Goloshumova, A.Y. Tarasova, M.S. Molokeev, L.I. Isaenko, A.F. Kurus, Single crystal growth and the electronic structure of Rb2Na(NO3)3: Experiment and theory, J. Solid State Chem. 294 (2021) 121910. https://doi.org/10.1016/j.jssc.2020.121910.

[51] C.A. Hunter, J.K.M. Sanders, The Nature of π-π Interactions, J. Am. Chem. Soc. 112 (1990) 5525–5534. https://doi.org/10.1021/ja00170a016.

[52] A.A.R. Watt, J.P. Bothma, P. Meredith, The supramolecular structure of melanin, Soft Matter. 5 (2009) 3754–3760. https://doi.org/10.1039/B902507C.

[53] A.B. Mostert, G.R. Hanson, T. Sarna, I.R. Gentle, B.J. Powell, P. Meredith, Hydration-Controlled X-Band EPR Spectroscopy: A Tool for Unravelling the Complexities of the Solid-State Free Radical in Eumelanin, J. Phys. Chem. B. 117 (2013) 4965–4972. https://doi.org/10.1021/jp401615e.

[54] K.Y. Ju, J. Kang, J.H. Chang, J.K. Lee, Clue to Understanding the Janus Behavior of Eumelanin: Investigating the Relationship between Hierarchical Assembly Structure of Eumelanin and Its Photophysical Properties, Biomacromolecules. 17 (2016) 2860–2872. https://doi.org/10.1021/acs.biomac.6b00686.

[55] S.K. Saha, H. Jain, A.C. Miller, R.K. Brow, XPS characterization of in situ prepared Ti/glass interfaces, Surf. Interface Anal. 24 (1996) 113–118. https://doi.org/10.1002/(SICI)1096-9918(199602)24:2<113::AID-SIA100>3.0.CO;2-C.

[56] M.I.N. da Silva, S.N. Dezidério, J.C. Gonzalez, C.F.O. Graeff, M.A. Cotta, Synthetic melanin thin films: Structural and electrical properties, J. Appl. Phys. 96 (2004) 5803–5807. https://doi.org/10.1063/1.1803629.

[57] G.S. Lorite, V.R. Coluci, M.I.N. da Silva, S.N. Dezidério, C.F.O. Graeff, D.S. Galvão, M. Cotta, Synthetic melanin films: Assembling mechanisms, scaling behavior, and structural properties, J. Appl. Phys. 99 (2006) 113511-1/113511-6.

Graphical abstract